ACS APPLIED MATERIALS & INTERFACES

www.acsami.org

Research Article

GO-Enhanced MXene Sediment-Based Inks Achieve Remarkable Oxidation Resistance and High Conductivity

Haofan Wen, Yunfa Si, Zibo Chen, Yitong Xin, Shaowen Cao, Cheng Chen,* Haoran Zu,* and Daping He*

Cite This: https://doi.org/10.1021/acsami.4c23060

Read Online

ACCESS | Metrics & More | Article Recommendations | Supporting Information

ABSTRACT: MXenes are emerging materials renowned for their exceptional conductivity, abundant functional groups, and excellent solution processability, making them highly promising as conductive-additive-free inks for flexible electronic devices. However, current preparation methods are hampered by low yields of MXene flakes so that substantial waste MXene sediments (MS) are generated. Here, we demonstrate a type of conductive ink with appropriate rheological properties, namely MG inks formulated using MS and graphene oxide (GO), for screen-printing frequency selective surface (FSS). GO facilitates interlayer interactions by covalently cross-linking with MXene flakes, resulting in a denser structure and significantly enhancing the conductivity of the best-performing MG-based ink to 849 S cm^{-1}. Additionally, GO serves as a binder to considerably improve the rheological properties of MS, thus enabling high-quality printing on various substrates. The close stacking of MS and GO not only improves the oxidation resistance but also maintains conductivity above 97% even after 60 days. Furthermore, the MG-based FSS produced via straightforward screen printing demonstrates excellent performance and retains its functionality after 90 days of operation. This MS-based ink formulation represents a strategy of "turning trash into treasure" and highlights the potential of MS for the next generation of electronic devices.

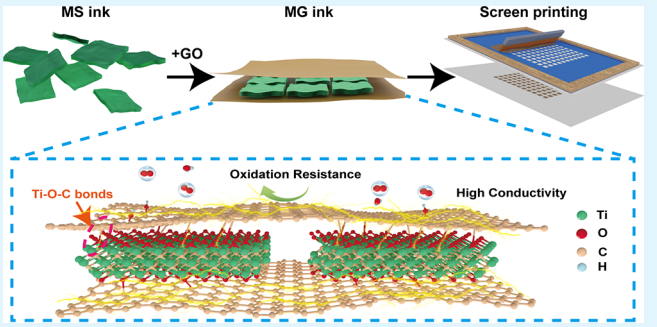

KEYWORDS: *MXene sediments, graphene oxides, oxidation resistance, high conductivity, frequency selective surface*

INTRODUCTION

With the rapid development of flexible printed electronics, there has been an increasing interest in functional conductive inks.[1,2] Flexible devices such as antennas, sensors, and supercapacitors can be printed by designing inks with various functionalities.[3−5] These devices require inks that are lightweight, corrosion-resistant, and cost-effective to meet practical application demands. Although traditional metallic materials have been widely used in conductive inks, they fall short owing to their high density, complicated processing, and susceptibility to corrosion, which do not fully meet the needs of flexible electronic devices.[6,7] Therefore, there is an urgent need to find new conductive inks that meet these requirements. Two-dimensional materials such as graphene and transition metal carbides/nitrides (MXenes) have been extensively explored due to their unique physical and chemical properties.[8−10] Among these, MXenes, a type of emerging material, exhibit significant advantages in forming stable aqueous conductive inks due to their excellent conductivity, solution processability, and abundant surface functional groups.[11,12] For example, high-performance wireless antennas and large-area fine logic circuits have been printed using MXene-based inks, demonstrating their promising potential as high-performance conductive inks for flexible electronic printing.[13−15]

Researchers primarily focus on preparing single-layer or multilayer MXenes to produce high-performance MXene inks.[16] Despite the increasing yields of single-layer MXenes in recent years,[17,18] some MXene sediments (MS) that are difficult to delaminate always remain at the bottom of the centrifuge tube.[19] These sediments, composed of unetched MAX, multilayer MXenes (*m*-MXenes), and small amounts of residual layered MXenes, are usually discarded as waste.[20,21] This practice not only increases the manufacturing cost of MXene inks but also results in a significant waste of materials, highlighting the necessity of recycling this "waste". It has been established that, like MXenes, the surface of MS is rich in hydrophilic functional groups including −OH, ═O, and −F. Besides, MS possesses relatively high conductivity, indicating

Received: December 31, 2024
Revised: February 5, 2025
Accepted: February 9, 2025

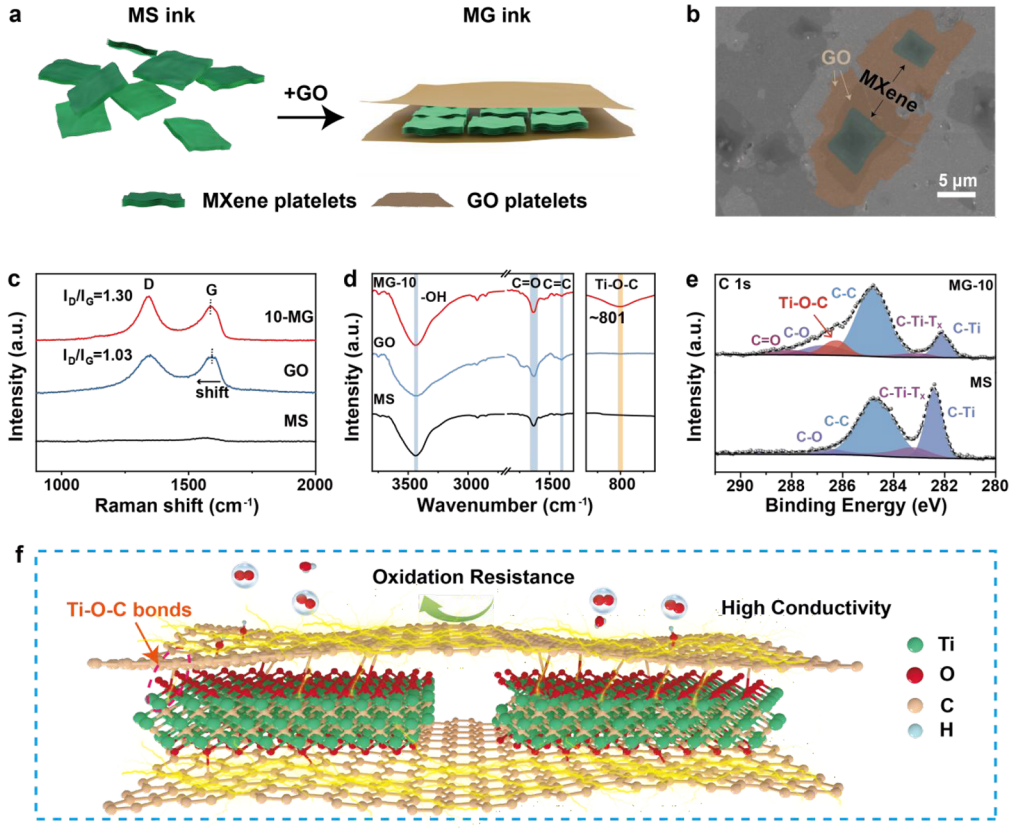

Figure 1. Characterization of the MG inks. (a) Schematic illustration for the manufacturing process of the MG inks. (b) SEM image of the MG flakes. Comparisons of (c) Raman spectroscopy spectra and (d) FT-IR spectra of MG-10, GO, and MS. (e) C 1s XPS spectra of MG-10 and MS nanosheets. (f) Mechanism of the Ti−O−C bonds.

its potential for ink applications.[22] Currently, some researchers have attempted to use MS-based inks to fabricate supercapacitors,[23,24] electromagnetic shielding films,[25] and photothermal conversion hydrogels.[26] However, the presence of unexfoliated multilayer MXenes and a small amount of MAX particles in MS severely hinder charge transfer and impact the ink's rheological properties, making it challenging to form highly conductive inks suitable for fine printing.[23] Additionally, similar to layered MXenes, MS has poor oxidation resistance, complicating the maintenance of stable performance in printed products over time.[27,28] Consequently, effectively recycling MS to transform it from waste into valuable materials is significant and remains a highly challenging task.

Herein, we fabricate a new type of MS-based ink featuring remarkable oxidation resistance and high conductivity. These inks exhibit enhanced rheological properties due to covalent cross-linking via Ti−O−C bonds between graphene oxide (GO) nanosheets and MS, leading to substantial improvements in MS/GO (MG) inks. The flexible MG printing pattern displays uniform boundaries and a complete surface, outperforming MS in terms of adhesion to various substrates. This superior adhesion facilitates the inks' ability to conform easily to different substrates. Moreover, the cross-linking between GO and MS effectively prevents the permeation of water and oxygen, thereby significantly enhancing the oxidation stability of the resulting inks. Remarkably, the conductivity of the printed patterns remains at approximately 97% after 60 days of exposure to ambient temperature and pressure. The conductivity of MG-based flexible electronic devices also shows a notable increase, reaching 849 S cm^{-1}, which is 1.63 times higher than that of MS (521 S cm^{-1}), probably due to interlayer interactions. Additionally, the denser structure of the MG ink reduced the printing thickness of the frequency selective surface (FSS) from 3.9 to 2.1 μm, while maintaining excellent performance. This FSS exhibits an effective bandwidth of 9.7 GHz within the 8−18 GHz range and only a 14% decrease in performance after 90 days. Combined with the simple and scalable preparation method, the high-performance, oxidation-resistant MG inks demonstrate significant potential for application in flexible printed electronic devices.

RESULTS AND DISCUSSION

Figure 1a schematically illustrates the preparation process for the MG inks. Initially, the sediment (MS) is obtained from the bottom after collecting the supernatant containing single-layer/few-layer MXene nanosheets via the minimally intensive layer delamination (MILD) method.[19] Scanning electron microscope (SEM) images reveal that the obtained MS comprises an unetched MAX phase and single-layer/multilayer MXene (Figure S1). To enhance the weak interaction and rheological properties of MS, large-sized GO (approximately 31 μm in size, Figure S2) is added as an effective binder to construct a stable ink (Figure 1a). This addition is crucial because the abundant surface functional groups on MXene nanosheets react with GO sheets, forming covalently cross-linked MXene-GO sheets (Figure 1b). The formation of Ti−O−C covalent bonds at the MXene/GO heterointerface is generally believed to occur through affinity substitution and dehydration reactions.[29−31] Specifically, GO platelets contain abundant

https://doi.org/10.1021/acsami.4c23060
ACS Appl. Mater. Interfaces XXXX, XXX, XXX−XXX

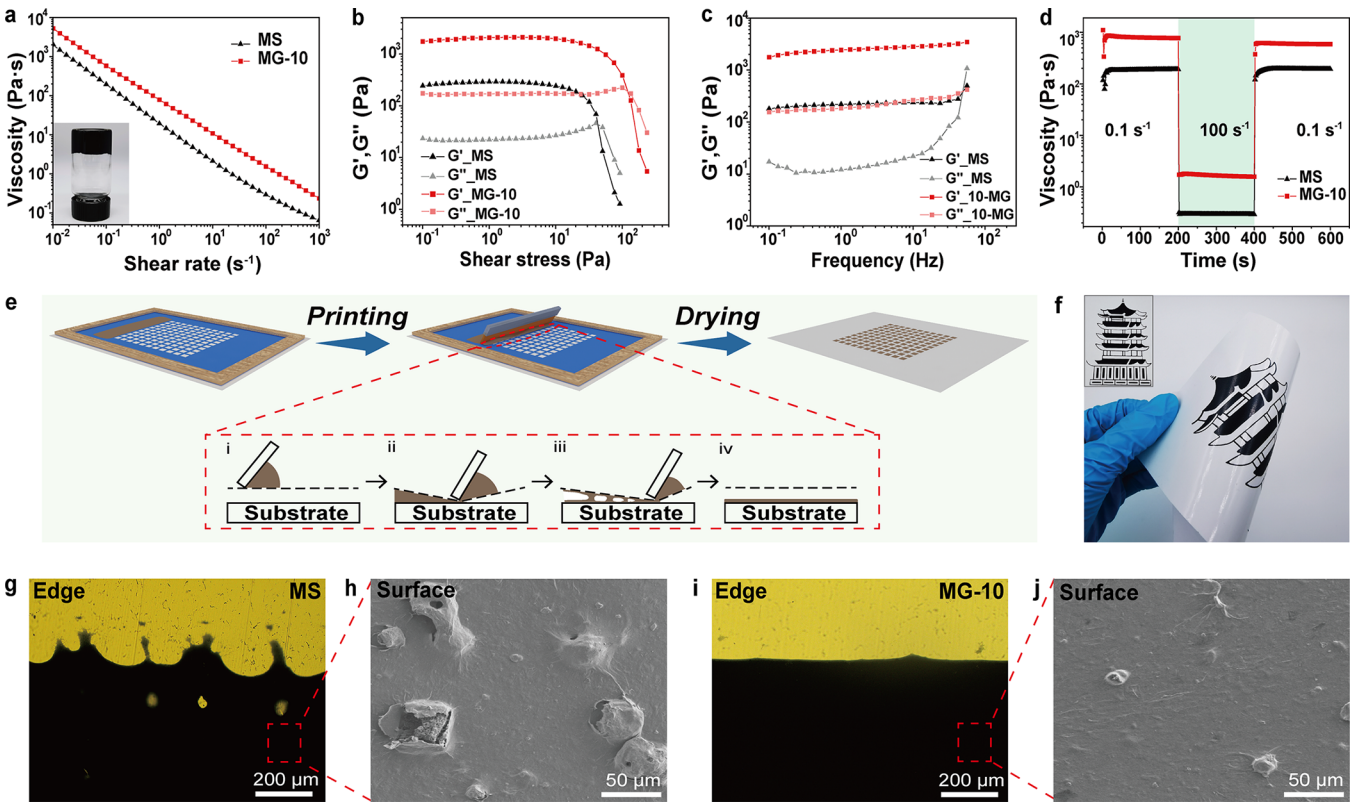

Figure 2. Properties and characterization of MG-10 and MS inks. (a) Ink viscosity versus shear rate. G' and G'' values of inks as functions of (b) shear stress and (c) frequency. (d) Thixotropy property of inks. (e) Schematic diagram of the screen-printing process. (f) Digital image of the MG-10 printed pattern on a glossy photo paper. Optical photographs and SEM images of printed patterns using (g, h) MS and (i, j) MG-10.

oxygen-containing functional groups (−COOH and −OH), which are initially protonated to form $-C{=}OH^+$ and $-C-OH_2^+$ species in H^+-containing solution. As the reaction proceeds, the $Ti-O^-$ bonds on MXene surfaces act as nucleophiles, attacking the $-C{=}OH^+$ and $-C-OH_2^+$ groups. This nucleophilic attack results in the elimination of H_2O molecules from GO platelets. Ultimately, this interfacial interaction leads to the formation of robust Ti−O−C covalent bonds between the MXene and GO components. Various analytical techniques have been utilized to confirm the formation of these Ti−O−C covalent bonds. The introduction of GO nanosheets results in a shift of the MS (002) peak from 5.78° to 6.11° and a decrease in interlayer spacing (Figure S3), which is attributed to the insertion of GO nanosheets into MS. Raman and FT-IR spectroscopy are employed to verify the existence of this covalent cross-linking. Raman spectroscopy (Figure 1c) reveals that the I_D/I_G intensity ratio of MG increases to 1.30 compared to 1.03 for the original GO, which is attributed to the reaction with MXene nanosheets. Additionally, the G band in MG (1585 cm^{-1}) exhibits a shift compared to that in GO (1592 cm^{-1}), indicating charge transfer between GO and MXene sheets, leading to the formation of Ti−O−C bonding.[31] Furthermore, as shown in Figures 1d and S4, a new peak at ∼801 cm^{-1} for MG-10 (feeding mass ratio (GO/MXene) = 10:90) indicates the formation of Ti−O−C bonds.[30] To further investigate the elemental composition and chemical states of MG and MS, XPS spectra were analyzed (Figure S5). Compared to MS, MG displays a new Ti−O−C peak at 286.2 eV in its high-resolution C 1s spectrum (Figure 1e), which is consistent with the Ti−O−C peak (531.2 eV) in the O 1s spectrum (Figure S6).[32,33] These results collectively demonstrate that incorporation of GO nanosheets into MS promotes the formation of Ti−O−C bonds. Interestingly, the formed GO protective nanolayer not only shields against the effects of water and oxygen but also serves as a pathway for electron transfer, reducing spatial resistance and enhancing the conductivity of the MG ink, which is beneficial for its application in printed electronics (Figure 1f).

On the other hand, the addition of GO sheets has significantly enhanced the rheological properties of the MS ink. As depicted in Figure 2a, both MS and MG-10 inks exhibit typical shear-thinning non-Newtonian fluid behavior, where the viscosity decreases with an increase in shear rate. This property is crucial for facilitating the extrusion of the ink through the screen mesh during the printing process. Notably, at a shear rate of 10 s^{-1}, the MG-10 ink demonstrates a substantially higher viscosity of 5312 Pa·s compared to 1974 Pa·s for the MS ink, thereby enabling the printing of finer patterns.[34] Figure 2b illustrates the variations in storage modulus (G') and loss modulus (G'') of MS and MG-10 inks as a function of shear stress. For both inks, G' significantly exceeds G'' at low shear stresses, indicating that a dominance of elastic behavior. Compared to MS, MG-10 exhibits a considerably higher G' value (1746 Pa) and yield stress (172 Pa), which ensures its suitability for high-precision printing applications.[35] Additionally, Figure 2c shows that, unlike the MS ink, which exhibits high-frequency instability, the G' of MG-10 consistently exceeds G'' across the entire frequency range, indicating its superior stability under varying frequencies. Furthermore, MG-10 manifests faster response and recovery rates at different shear rates compared to MS (Figure

https://doi.org/10.1021/acsami.4c23060
ACS Appl. Mater. Interfaces XXXX, XXX, XXX−XXX

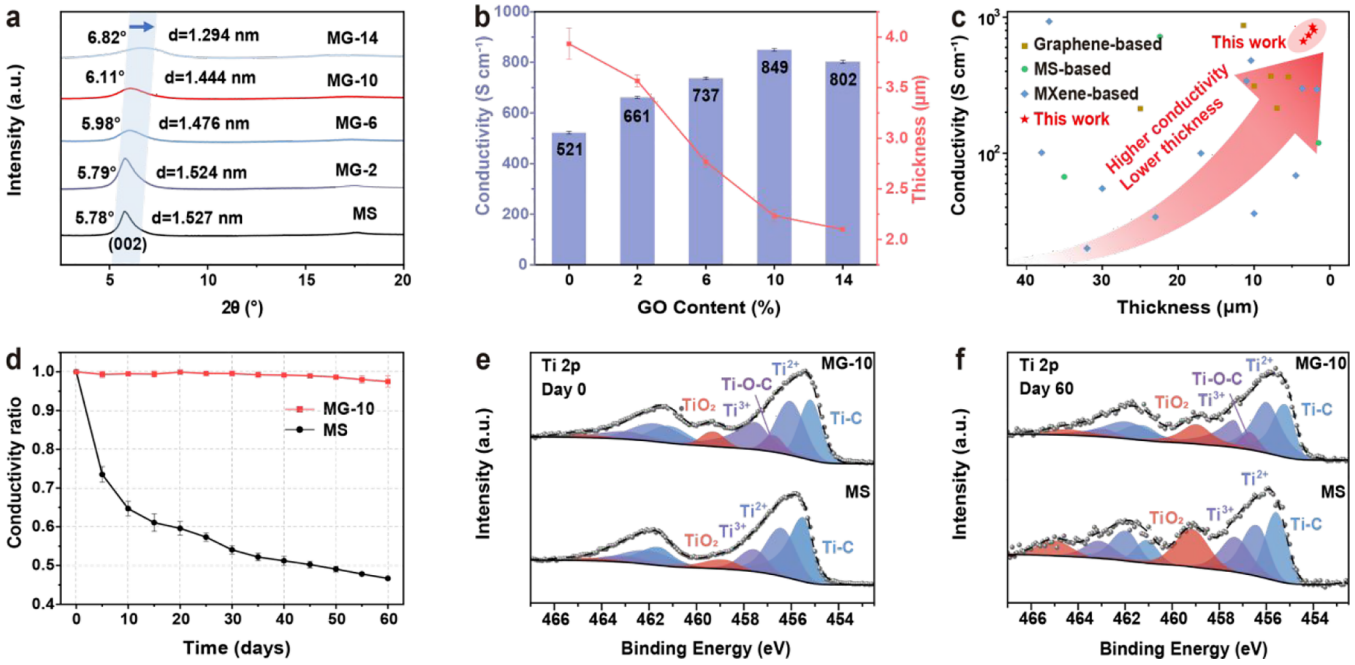

Figure 3. (a) XRD patterns of MG with different GO contents. (b) Printing thickness and conductivity of MG films with different GO contents. (c) Comparison of conductivity and thickness of printed products with reported 2D material inks. (d) Conductivity retention rates of MG-10 and MS as a function of exposure time in air. (e, f) Ti 2p XPS spectra of MG-10 and MS films on (e) day 0 and (f) day 60.

2d). Altogether, the MG-10 ink exhibits higher viscosity, higher elasticity, and broader applicability, making it more suitable for high-precision and rapid printing than the MS ink.

Based on the superior rheological properties of MG-10, we further demonstrate its applicability and advantages in screen printing technology. The fabrication process of the FSS via screen printing is illustrated in Figure 2e. Owing to its improved rheological properties over MS, the MG-10 ink can achieve high-precision printing on various flexible substrates such as polyimide (PI), cardboard, paper, copper foil, and glossy photo paper (Figures 2f and S7). Furthermore, the printed patterns maintain strong adhesion to the substrate even under bending conditions, exhibiting no structural degradation or delamination (Figure 2f). In contrast, MS struggles to pass uniformly through the mesh, resulting in edge blurring or uneven line widths when printing fine patterns such as stripes (Figures S8 and S9). Figure 2g–j shows the edge optical photographs and SEM image of the printed pattern using MS and MG-10, respectively. The MG-10 ink produces patterns with superior resolution and print quality, while MS leads to numerous surface defects, low resolution, and uneven edges. SEM images reveal that MS-based patterns have a rough surface due to the presence of numerous particles, including unetched MAX and m-MXene. In contrast, the surface of MG-10-based patterns is relatively smooth because the incorporated GO sheets effectively encapsulate most of the particles through chemical cross-linking. This is consistent with the conclusions drawn from optical profilometry (Figure S10). Therefore, MG-10 holds excellent potential for high-precision printing of various flexible electronic devices across a wide range of applications.

Subsequently, further characterization analyses have been conducted to investigate the impact of GO content on the printed products of the MG inks. As observed from the XRD pattern (Figures 3a and S11), the interlayer spacing decreases from 1.527 to 1.294 nm as the GO content is enhanced. This reduction in spacing correlates with a decrease in printing thickness to reaching a minimum value of 2.1 μm (Figure S12), which is attributed to enhanced interlayer interactions after GO addition to provide a denser structure. These interactions facilitate electron transport, thereby achieving high conductivity in printed devices. The conductivity increased with the GO content and a maximum value of 849 S cm^{-1} is achieved at 10% GO content, which makes a 163% improvement over MS (521 S cm^{-1}). As demonstrated, a circuit drawn with MG-10 can easily illuminate bulbs (Figure S13). Notably, as illustrated in Figure 3c and Table S1, the electrical conductivity of MG-10 surpasses that of existing MS-based printed inks[24,36−38] and even outperforms representative inks prepared using d-$Ti_3C_2T_x$.[39−43] Moreover, GO flakes not only enhance the electrical conductivity of MG-10 through chemical cross-linking but also improve its oxidation resistance by acting as a barrier layer against oxygen and water molecules.[44,45] This protective effect is evident in the MG-10 film, which maintained up to 97% of its initial conductivity after 60 days of air exposure. Conversely, the conductivity of the MS film decreased to only 46% of its initial value over the same period (Figure 3d). The superior performance of the MG-10 film is attributed to its dense structure and the effective inhibition of oxygen and water penetration with the incorporation of GO. To further investigate the oxidation resistance of the films prepared with MG and MS inks, XPS measurements were conducted. For the Ti 2p spectrum of MG-10, peaks at 459.3 and 465 eV correspond to the Ti−O bonds in the Ti $2p_{3/2}$ and Ti $2p_{1/2}$ orbitals, respectively. After 60 days, the peaks associated with Ti−O in the MG-10 ink showed only minor change to 459.0 and 464.6 eV, respectively. In contrast, the proportion of Ti−O bonds in the MS film increased significantly after 60 days, indicating the onset of transformation into TiO_2. These findings underscore the enhanced oxidation resistance provided by GO in the MG-10 film.

https://doi.org/10.1021/acsami.4c23060
ACS Appl. Mater. Interfaces XXXX, XXX, XXX−XXX

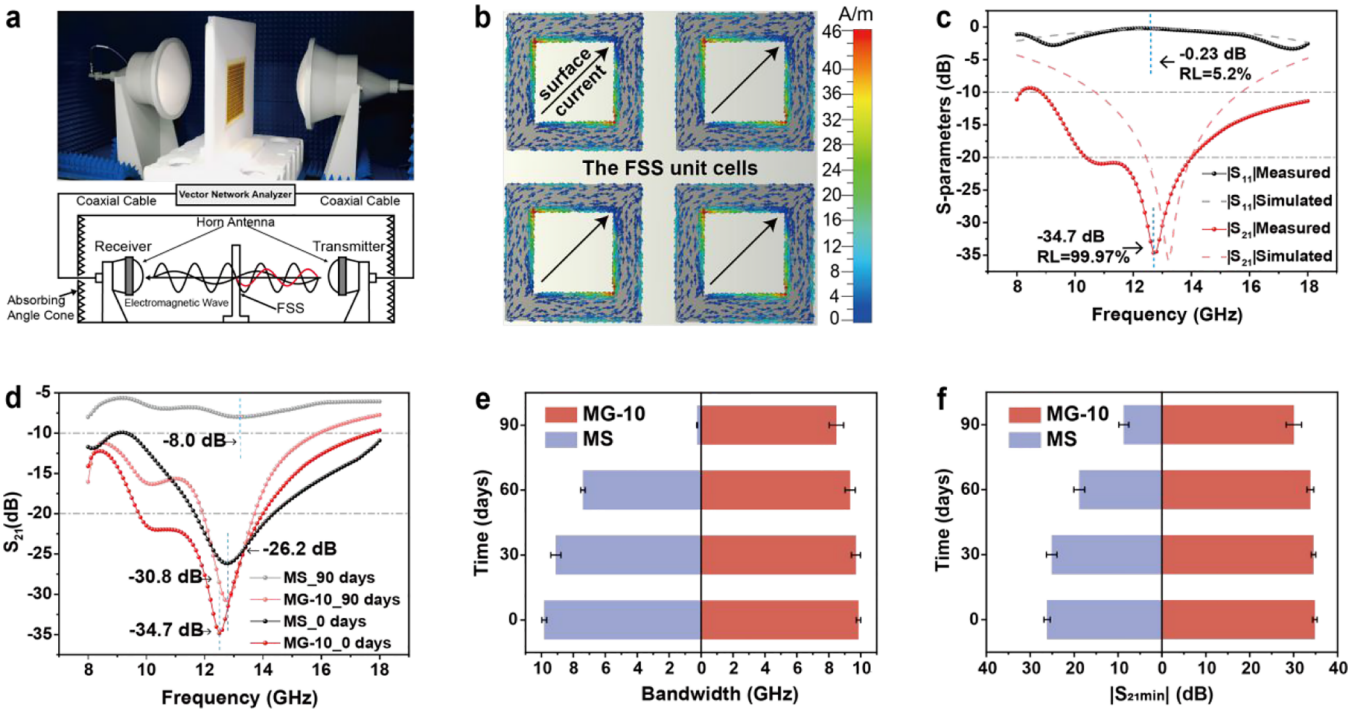

Figure 4. (a) Schematic illustration of the measurement environment and function of the FSS. (b) Surface current distributions of the FSS unit cells. (c) Simulated and measured *S* parameters of the MG-10-based FSS. (d–f) Comparison of MG-10- and MS-based FSS at different times: (d) S_{21} parameters, (e) bandwidth, and (f) $|S_{21\ min}|$.

The MG-10 ink, characterized by its excellent rheological properties, high conductivity, and good stability, demonstrates significant potential for scalable printing in flexible electronic devices. Leveraging these advantages, we designed an MG-10-based FSS and compared its performance with an FSS fabricated using the MS ink. The FSS model and specific parameters are detailed in Figure S14. We printed the FSS on a PI substrate, as illustrated in Figure 4a, and conducted measurements using a vector network analyzer in an anechoic chamber. When electromagnetic waves transmitted by a horn antenna encounter the FSS, an induced current is generated on the surface of the FSS unit cells. This induced current flows diagonally along the FSS unit cells, forming a resonant circuit (Figure 4b). At the resonant frequency, the standing wave states in these current paths lead to strong reflection of the electromagnetic waves for both vertical and horizontal polarizations. Through this mechanism, the FSS effectively achieves reflection shielding of electromagnetic waves at specific resonant frequencies, functioning as a bandstop filter. Moreover, by altering the parameters or materials of the FSS elements, the resonant frequency can be adjusted to meet the requirements of different applications across various frequencies.[46,47] The electrical conductivity and rheological properties of the ink are pivotal in determining FSS performance. Higher electrical conductivity minimizes ohmic losses, thereby enhancing the FSS's operational stability. Conversely, lower electrical conductivity can lead to a drift in resonant frequency due to increased resistive dissipation. Additionally, enhanced rheological properties facilitate better substrate integration, which is critical for avoiding common fabrication defects such as pattern delamination, microcrack formation, and loss of edge definition. These improvements are vital for maintaining the precision of the FSS's periodic architecture.

The simulated and measured *S* parameters of the MG-based FSS are depicted in Figure 4c. Within the frequency range of 8–18 GHz, the return loss (S_{11}) approaches 0 dB, while the insertion loss (S_{21}) consistently remains below −10 dB across the entire frequency band, indicating a bandwidth of 9.8 GHz. This performance signifies that the FSS achieves a reflection shielding efficiency of over 90% within the 8–18 GHz range and reaches up to 99% shielding efficiency (below −20 dB) in the 9.7–14 GHz range, meeting commercial application requirements. The resonant frequency of this FSS is observed at 12.5 GHz, where the minimum S_{21} value of −34.9 dB is achieved, corresponding to a reflection loss (RL) of 99.97%. Overall, the MG-10-based FSS outperforms the MS-based FSS and is even comparable to the FSS prepared using d-MXene, as shown in Figure S15. To evaluate the stability of the device, we exposed the FSS to air for 90 days. After this period, the S_{21} parameter of the MG-10-based FSS in the 8–18 GHz range showed only slight changes, manifesting minimal performance degradation (Figures 4d and S16). In contrast, the S_{21} parameter of the MS-based FSS was above −10 dB, indicating that its shielding performance almost disappeared. Further comparisons were made on the bandwidth and minimum S_{21} ($S_{21\ min}$) versus time. As shown in Figure 4e, the bandwidth of the MG-10-based FSS at 30, 60, and 90 days was 98.4, 94.7, and 86% of the initial value, respectively. Conversely, the performance of the MS-based FSS declined rapidly, with the bandwidth at 60 days reduced to only 75.3% of the initial value and nearly disappearing by 90 days. Correspondingly, the $S_{21\ min}$ of the MS-based FSS sharply declined starting from the 60th day, dropping to only 31.8% of its original value by the 90th day (Figure 4f). In contrast, the MG-10-based FSS maintained its $S_{21\ min}$ at over 85% throughout the same period. These results demonstrate that flexible electronic devices printed with the MG-10 ink exhibit excellent performance and

https://doi.org/10.1021/acsami.4c23060
ACS Appl. Mater. Interfaces XXXX, XXX, XXX−XXX

stability, making it suitable not only for FSS but also showing potential in other application fields.

CONCLUSIONS

In summary, we have developed a highly conductive and stable MG ink suitable for screen printing flexible FSS. By incorporating GO nanosheets into MS, we significantly enhanced the inks' conductivity and protected the MXene sheets from water and oxygen by strengthening interlayer interactions. This improvement in the MG inks demonstrates excellent rheological properties, allowing for precise printing on various substrates with strong adhesion. Adjusting the GO content enables the production of printed products with varying thicknesses and conductivities, maintaining above 90% of conductivity over 90 days. Notably, the FSS prepared with the MG-10 ink exhibits an effective bandwidth of up to 9.8 GHz within the 8−18 GHz range and retains 86% of this bandwidth even after 90 days of storage. Compared to the MS-based FSS, the MG-10-based FSS shows significantly enhanced comprehensive performance. Utilizing "MXene waste" as a raw material for preparing MS-based conductive inks offers advantages such as zero waste, scalability, and low cost. Owing to their high conductivity, stability, and broad applicability, the MG-10 ink holds great potential for the printing of flexible electronic devices.

METHODS

Materials. LiF was purchased from Aladdin (China). HCl was purchased from Sinopharm Chemical Reagent Co., Ltd. Ti_3AlC_2 MAX powder was obtained from Jilin 11 Technology Co., Ltd. GO (4 wt %, sheet diameter of ∼30 μm) was purchased from Wuhan Hanene Technology Co., Ltd.

Preparation of $Ti_3C_2T_x$ MXene Sediments. $Ti_3C_2T_x$ MXene was prepared by etching Ti_3AlC_2 powder (400 mesh) with a LiF/HCl solution, following a previously reported method.[48] Specifically, LiF (16 g) was dissolved in 9 M HCl (200 mL) within a Teflon vessel and stirred for 20 min. Subsequently, Ti_3AlC_2 powder (10 g) was slowly added to the reaction vessel, and the suspension was stirred at 50 °C for 36 h. The resulting dispersion was then repeatedly rinsed with fresh deionized water through centrifugation at 3000 rpm for 5 min until the supernatant transitioned from black (indicating self-delamination) to transparent. Finally, the precipitate collected at the bottom of the centrifuge tube, typically discarded, was obtained as the required MS.

Preparation of the MS/GO (MG) Inks. To formulate the MG, MS was mixed with GO at various mass ratios using a planetary mixer (2000 rpm, 15 min) to form uniform inks. Among them, the concentrations of MS and GO dispersions were 80 and 40 mg/mL, respectively. According to the different mass fractions of GO, they are named MG-2, MG-4, MG-6, MG-8, MG-10, MG-12, and MG-14, respectively.

Preparation of Screen-Printed FSS. A screen printer (SY-500P) equipped with a custom-made 60-mesh polyethylene terephthalate (PET) mask was employed for the printing process. During printing, a specific quantity of an MG ink was applied onto the screen mesh, followed by swift pattern scraping with a squeegee to transfer the ink onto diverse substrates such as PI, paper, copper foil, and cardboard. After a natural drying period of 10 min, finely printed patterns were obtained on the substrates.

Characterization. The morphology and microstructures were examined using a ZEISS Crossbeam 350 scanning electron microscope and Olympus IX73 optical microscope. XRD patterns were recorded using Cu Kα radiation from a Rigaku Miniflex 600 apparatus. XPS measurements were performed with an Escalab 250Xi Spectrophotometer. The rheological behaviors of the inks were characterized at 25 °C using a Malvern Kinexus rheometer. FT-IR spectra were collected on a Bruker Invenio-S spectrometer. Raman spectra were recorded at room temperature using a DXR Raman Microscope (American Thermo Electron) with 532 nm-wavelength laser excitation. Electrical conductivities were measured using an RTS-9 four-probe resistivity meter (China). The electromagnetic interference shielding performances of the FSS were measured on a Ceyear 3672C vector network analyzer within the 8−18 GHz range based on a waveguide method.

ASSOCIATED CONTENT

Supporting Information

The Supporting Information is available free of charge at https://pubs.acs.org/doi/10.1021/acsami.4c23060.

Additional SEM images, XRD patterns, FT-IR spectroscopy analysis, and XPS spectra for the GO, MS, and MG samples presented in this study; size distribution for m-MXene and GO nanosheets; printing effect display; FSS model and unit cell parameters; and comparison of S_{21} parameters (PDF)

AUTHOR INFORMATION

Corresponding Authors

Cheng Chen − *Sanya Science and Education Innovation Park of Wuhan University of Technology, Sanya 572000, China; State Key Laboratory of Advanced Technology for Materials Synthesis and Processing, Wuhan University of Technology, Wuhan 430070, P. R. China;* orcid.org/0000-0001-5439-5421; Email: chengchen@whut.edu.cn

Haoran Zu − *School of Information Engineering, Wuhan University of Technology, Wuhan 430070, China;* Email: zuhr@whut.edu.cn

Daping He − *Sanya Science and Education Innovation Park of Wuhan University of Technology, Sanya 572000, China; State Key Laboratory of Advanced Technology for Materials Synthesis and Processing, Wuhan University of Technology, Wuhan 430070, P. R. China; Hubei Engineering Research Center of RF-Microwave Technology and Application, Wuhan University of Technology, Wuhan 430070, China;* orcid.org/0000-0002-0284-4990; Email: hedaping@whut.edu.cn

Authors

Haofan Wen − *Sanya Science and Education Innovation Park of Wuhan University of Technology, Sanya 572000, China*

Yunfa Si − *Sanya Science and Education Innovation Park of Wuhan University of Technology, Sanya 572000, China*

Zibo Chen − *Sanya Science and Education Innovation Park of Wuhan University of Technology, Sanya 572000, China*

Yitong Xin − *State Key Laboratory of Advanced Technology for Materials Synthesis and Processing, Wuhan University of Technology, Wuhan 430070, P. R. China*

Shaowen Cao − *Sanya Science and Education Innovation Park of Wuhan University of Technology, Sanya 572000,*

https://doi.org/10.1021/acsami.4c23060
ACS Appl. Mater. Interfaces XXXX, XXX, XXX−XXX

China; State Key Laboratory of Advanced Technology for Materials Synthesis and Processing, Wuhan University of Technology, Wuhan 430070, P. R. China; orcid.org/0000-0003-4556-2341

Complete contact information is available at: https://pubs.acs.org/10.1021/acsami.4c23060

Author Contributions

H.W. and Y.S. contributed equally to this work. The manuscript was written through the contributions of all authors. All authors have approved the final version of the manuscript.

Notes

The authors declare no competing financial interest.

■ ACKNOWLEDGMENTS

This work is supported by Sanya Science and Education Innovation Park of Wuhan University of Technology (No: 2022KF0013), the Natural Science Foundation of Hainan Province of China (No. 623MS068), the PhD Scientific Research and Innovation Foundation of Sanya Yazhou Bay Science and Technology City (No. HSPHDSRF-2023-03-012), the National Natural Science Foundation of China (Nos. 22279097, 62401413), and the Fundamental Research Funds for the Central Universities (WUT: 2024IVA031).

■ REFERENCES

(1) Kamyshny, A.; Magdassi, S. Conductive Nanomaterials for 2D and 3D Printed Flexible Electronics. *Chem. Soc. Rev.* **2019**, *48*, 1712−1740.

(2) Zhang, Y. Z.; Wang, Y.; Cheng, T.; Yao, L. Q.; Li, X.; Lai, W. Y.; Huang, W. Printed Supercapacitors: Materials, Printing and Applications. *Chem. Soc. Rev.* **2019**, *48*, 3229−3264.

(3) Liu, H.; Zhang, H.; Han, W.; Lin, H.; Li, R.; Zhu, J.; Huang, W. 3D Printed Flexible Strain Sensors: From Printing to Devices and Signals. *Adv. Mater.* **2021**, *33*, No. e2004782.

(4) Yang, W.; Cheng, X.; Guo, Z.; Sun, Q.; Wang, J.; Wang, C. Design, Fabrication and Applications of Flexible RFID Antennas Based on Printed Electronic Materials and Technologies. *J. Mater. Chem. C* **2023**, *11*, 406−425.

(5) Lai, M.; Zhao, C.; Wang, D.; Gao, R.; Cai, P.; Sun, L.; He, Q.; Peng, H.; Zhang, H.; Xu, F.; et al. Significantly Enhanced Oxidation Resistance and Electrochemical Performance of Hydrothermal $Ti_3C_2T_x$ MXene and Tannic Acid Composite for High-Performance Flexible Supercapacitors. *ACS Appl. Mater. Interfaces* **2024**, *16*, 55555−55568.

(6) Pinilla, S.; Coelho, J.; Li, K.; Liu, J.; Nicolosi, V. Two-dimensional material inks. *Nat. Rev. Mater.* **2022**, *7*, 717−735.

(7) Li, P.; Zhang, Y.; Zheng, Z. Polymer-Assisted Metal Deposition (PAMD) for Flexible and Wearable Electronics: Principle, Materials, Printing, and Devices. *Adv. Mater.* **2019**, *31*, No. e1902987.

(8) Hu, G.; Kang, J.; Ng, L. W. T.; Zhu, X.; Howe, R. C. T.; Jones, C. G.; Hersam, M. C.; Hasan, T. Functional Inks and Printing of Two-dimensional Materials. *Chem. Soc. Rev.* **2018**, *47*, 3265−3300.

(9) Ahmed, A.; Sharma, S.; Adak, B.; Hossain, M. M.; LaChance, A. M.; Mukhopadhyay, S.; Sun, L. Two-dimensional MXenes: New Frontier of Wearable and Flexible Electronics. *InfoMat* **2022**, *4*, No. e12295.

(10) Tran, T. S.; Dutta, N. K.; Choudhury, N. R. Graphene Inks for Printed Flexible Electronics: Graphene Dispersions, Ink Formulations, Printing Techniques and Applications. *Adv. Colloid Interface Sci.* **2018**, *261*, 41−61.

(11) Wei, Y.; Zhang, P.; Soomro, R. A.; Zhu, Q.; Xu, B. Advances in the Synthesis of 2D MXenes. *Adv. Mater.* **2021**, *33*, No. 2103148.

(12) Abdolhosseinzadeh, S.; Jiang, X.; Zhang, H.; Qiu, J.; Zhang, C. Perspectives on Solution Processing of Two-Dimensional MXenes. *Mater. Today* **2021**, *48*, 214−240.

(13) Zheng, S.; Wang, H.; Das, P.; Zhang, Y.; Cao, Y.; Ma, J.; Liu, S. F.; Wu, Z. S. Multitasking MXene Inks Enable High-Performance Printable Microelectrochemical Energy Storage Devices for All-Flexible Self-Powered Integrated Systems. *Adv. Mater.* **2021**, *33*, No. 2005449.

(14) Chen, S.; Fu, H.; Si, Y.; Liu, X.; Wang, Z.; Duan, Y.; Zhang, Z.; Feng, H.; Zhao, X.; He, D. Size Effect Enabling Additive-Free MXene Ink with Ultrahigh Conductivity for Screen Printing of Wireless Electronics. *Nano Res.* **2023**, *16*, 11012−11017.

(15) Abdolhosseinzadeh, S.; Schneider, R.; Jafarpour, M.; Merlet, C.; Nüesch, F.; Zhang, C.; Heier, J. MXene Inks for High-Throughput Printing of Electronics. *Adv. Electron. Mater.* **2024**, *11*, No. 2400170.

(16) Wu, Z.; Shang, T.; Deng, Y.; Tao, Y.; Yang, Q. H. The Assembly of MXenes from 2D to 3D. *Adv. Sci.* **2020**, *7*, No. 1903077.

(17) Zhang, Q.; Fan, R.; Cheng, W.; Ji, P.; Sheng, J.; Liao, Q.; Lai, H.; Fu, X.; Zhang, C.; Li, H. Synthesis of Large-Area MXenes with High Yields through Power-Focused Delamination Utilizing Vortex Kinetic Energy. *Adv. Sci.* **2022**, *9*, No. 2202748.

(18) Huang, X.; Huang, J.; Yang, J.; Yang, D.; Li, T.; Dong, A. High-Yield Exfoliation of Large MXene with Flake Sizes over 10 μm Using Edge-Anchored Carbon Nanotubes. *Adv. Funct. Mater.* **2023**, *33*, No. 2303003.

(19) Huang, P.; Ying, H.; Zhang, S.; Han, W.-Q. Recent Advances and Perspectives of MXene Sediment: Composition, Morphology, Properties and Applications. *Coord. Chem. Rev.* **2024**, *515*, No. 215964.

(20) Zheng, S.; Wu, N.; Liu, Y.; Wu, Q.; Yang, Y.; Li, B.; Hu, C.; Liu, J.; Zeng, Z. Multifunctional Flexible, Crosslinked Composites Composed of Trashed MXene Sediment with High Electromagnetic Interference Shielding Performance. *Adv. Compos. Hybrid Mater.* **2023**, *6*, 161.

(21) Yang, Y.; Wu, N.; Li, B.; Liu, W.; Pan, F.; Zeng, Z.; Liu, J. Biomimetic Porous MXene Sediment-Based Hydrogel for High-Performance and Multifunctional Electromagnetic Interference Shielding. *ACS Nano* **2022**, *16*, 15042−15052.

(22) Huang, W.; Hu, L.; Tang, Y.; Xie, Z.; Zhang, H. Recent Advances in Functional 2D MXene-Based Nanostructures for Next-Generation Devices. *Adv. Funct. Mater.* **2020**, *30*, No. 2005223.

(23) Yuan, M.; Wang, L.; Liu, X.; Du, X.; Zhang, G.; Chang, Y.; Xia, Q.; Hu, Q.; Zhou, A. 3D Printing Quasi-Solid-State Micro-Supercapacitors with Ultrahigh Areal Energy Density Based on High Concentration MXene Sediment. *Chem. Eng. J.* **2023**, *451*, No. 138686.

(24) Abdolhosseinzadeh, S.; Schneider, R.; Verma, A.; Heier, J.; Nuesch, F.; Zhang, C. J. Turning Trash into Treasure: Additive Free MXene Sediment Inks for Screen-Printed Micro-Supercapacitors. *Adv. Mater.* **2020**, *32*, No. 2000716.

(25) Liu, Y.; Wu, N.; Zheng, S.; Yang, Y.; Li, B.; Liu, W.; Liu, J.; Zeng, Z. From MXene Trash to Ultraflexible Composites for Multifunctional Electromagnetic Interference Shielding. *ACS Appl. Mater. Interfaces* **2022**, *14*, 50120−50128.

(26) Wang, T.; Li, M.; Xu, H.; Wang, X.; Jia, M.; Hou, X.; Gao, S.; Liu, Q.; Yang, Q.; Tian, M.; et al. MXene Sediment-Based Poly(vinyl alcohol)/Sodium Alginate Aerogel Evaporator with Vertically Aligned Channels for Highly Efficient Solar Steam Generation. *Nano-Micro Lett.* **2024**, *16*, 220.

(27) Cao, F.; Zhang, Y.; Wang, H.; Khan, K.; Tareen, A. K.; Qian, W.; Zhang, H.; Agren, H. Recent Advances in Oxidation Stable Chemistry of 2D MXenes. *Adv. Mater.* **2022**, *34*, No. e2107554.

(28) Deng, S.; Guo, T.; Nüesch, F.; Heier, J.; Zhang, C. Stable MXene Dough with Ultrahigh Solid Fraction and Excellent Redispersibility toward Efficient Solution Processing and Industrialization. *Adv. Sci.* **2023**, *10*, No. 2300660.

(29) Li, B.; Wu, N.; Yang, Y.; Pan, F.; Wang, C.; Wang, G.; Xiao, L.; Liu, W.; Liu, J.; Zeng, Z. Graphene Oxide-Assisted Multiple Cross-Linking of MXene for Large-Area, High-Strength, Oxidation-

Resistant, and Multifunctional Films. *Adv. Funct. Mater.* **2022**, *33*, No. 2213357.
(30) Qiang, Y.; Ran, B.; Li, M.; Xu, Q.; Peng, J. GO-Functionalized MXene Towards Superior Anti-Corrosion Coating. *J. Colloid Interface Sci.* **2023**, *642*, 595−603.
(31) Zhou, T.; Wu, C.; Wang, Y.; Tomsia, A. P.; Li, M.; Saiz, E.; Fang, S.; Baughman, R. H.; Jiang, L.; Cheng, Q. Super-tough MXene-functionalized graphene sheets. *Nat. Commun.* **2020**, *11*, 2077.
(32) Li, H.; Hou, Y.; Wang, F.; Lohe, M. R.; Zhuang, X.; Niu, L.; Feng, X. Flexible All-Solid-State Supercapacitors with High Volumetric Capacitances Boosted by Solution Processable MXene and Electrochemically Exfoliated Graphene. *Adv. Energy Mater.* **2016**, *7*, No. 1601847.
(33) Yu, D.; Guo, K.; Hou, F.; Zhang, Y.; Ye, X.; Zhang, Y.; Ji, P.; Khalilov, U.; Wang, G.; Zhang, X. Ti horizontal line O horizontal line C Bonding at 2D Heterointerfaces of 3D Composites for Fast Sodium Ion Storage at High Mass Loading Level. *Small* **2024**, *20*, No. e2312167.
(34) Yu, L.; Fan, Z.; Shao, Y.; Tian, Z.; Sun, J.; Liu, Z. Versatile N-Doped MXene Ink for Printed Electrochemical Energy Storage Application. *Adv. Energy Mater.* **2019**, *9*, No. 1901839.
(35) Zhang, Y.; Zhu, Y.; Zheng, S.; Zhang, L.; Shi, X.; He, J.; Chou, X.; Wu, Z.-S. Ink Formulation, Scalable Applications and Challenging Perspectives of Screen Printing for Emerging Printed Micro-electronics. *J. Energy Chem.* **2021**, *63*, 498−513.
(36) Li, B.; Wu, N.; Wu, Q.; Yang, Y.; Pan, F.; Liu, W.; Liu, J.; Zeng, Z. From "100%" Utilization of MAX/MXene to Direct Engineering of Wearable, Multifunctional E-Textiles in Extreme Environments. *Adv. Funct. Mater.* **2023**, *33*, No. 2307301.
(37) Wu, C.-W.; Unnikrishnan, B.; Chen, I. W. P.; Harroun, S. G.; Chang, H.-T.; Huang, C.-C. Excellent Oxidation Resistive MXene Aqueous Ink for Micro-Supercapacitor Application. *Energy Storage Mater.* **2020**, *25*, 563−571.
(38) Zhou, J.; Shi, D.; Wang, Y.; Dong, W.; Chen, M. Multifunctional MXene Sediment-Based Composite Film for Electro-magnetic Interference Shielding and Joule Heating. *Compos. Commun.* **2023**, *37*, No. 101432.
(39) Zhang, C. J.; Park, S. H.; Seral-Ascaso, A.; Barwich, S.; McEvoy, N.; Boland, C. S.; Coleman, J. N.; Gogotsi, Y.; Nicolosi, V. High Capacity Silicon Anodes Enabled by MXene Viscous Aqueous ink. *Nat. Commun.* **2019**, *10*, 849.
(40) Nguyen, V.-T.; Nguyen, Q.-D.; Min, B. K.; Yi, Y.; Choi, C.-G. $Ti_3C_2T_x$ MXene/Carbon Nanotubes/Waterborne Polyurethane Based Composite Ink for Electromagnetic Interference Shielding and Sheet Heater Applications. *Chem. Eng. J.* **2022**, *430*, No. 133171.
(41) Tian, W.; VahidMohammadi, A.; Reid, M. S.; Wang, Z.; Ouyang, L.; Erlandsson, J.; Pettersson, T.; Wagberg, L.; Beidaghi, M.; Hamedi, M. M. Multifunctional Nanocomposites with High Strength and Capacitance Using 2D MXene and 1D Nanocellulose. *Adv. Mater.* **2019**, *31*, No. e1902977.
(42) Wu, H.; Xie, Y.; Ma, Y.; Zhang, B.; Xia, B.; Zhang, P.; Qian, W.; He, D.; Zhang, X.; Li, B. W. Aqueous MXene/Xanthan Gum Hybrid Inks for Screen-Printing Electromagnetic Shielding, Joule Heater, and Piezoresistive Sensor. *Small* **2022**, *18*, No. e2107087.
(43) Deng, Z.; Li, L.; Tang, P.; Jiao, C.; Yu, Z. Z.; Koo, C. M.; Zhang, H. B. Controllable Surface-Grafted MXene Inks for Electro-magnetic Wave Modulation and Infrared Anti-Counterfeiting Applications. *ACS Nano* **2022**, *16*, 16976−16986.
(44) Yang, X.; Wang, Q.; Zhu, K.; Ye, K.; Wang, G.; Cao, D.; Yan, J. 3D Porous Oxidation-Resistant MXene/Graphene Architectures Induced by In Situ Zinc Template toward High-Performance Supercapacitors. *Adv. Funct. Mater.* **2021**, *31*, No. 2101087.
(45) Xing, Z.; Si, Y.; Jin, H.; Zhang, B.; Chen, Z.; Fang, J.; Zhang, J.; Chen, C.; He, D. Mixed-Sized Graphene Oxides Induce Highly Densified MXene-Based Films with High Conductivity and Excep-tional Stability. *Adv. Mater. Technol.* **2024**, *9*, No. 2302098.
(46) Munk, B. A.; *Frequency Selective Surfaces: Theory and Design*; Wiley Interscience, 2000.
(47) Wu, T. K. *Frequency Selective Surface and Grid Array*; Wiley, 1995.
(48) Si, Y.; Jin, H.; Zhang, Q.; Xu, D.; Xu, R.; Ding, A.; Liu, D. Roll-to-roll processable MXene-rGO-PVA Composite Films with En-hanced Mechanical Properties and Environmental Stability for Electromagnetic Interference Shielding. *Ceram. Int.* **2022**, *48*, 24898−24905.

https://doi.org/10.1021/acsami.4c23060
ACS Appl. Mater. Interfaces XXXX, XXX, XXX−XXX